# Estimation of Ionospheric TEC and Faraday Rotation for L-Band SAR

Michael Jehle, Maurice Rüegg, David Small, Erich Meier and Daniel Nüesch

Remote Sensing Laboratories, University of Zürich, CH-8057 Zürich, Switzerland

## ABSTRACT

Spaceborne synthetic aperture radar (SAR) systems are used to measure geo- and biophysical parameters of the earth's surface, e.g. for agriculture, forestry and land subsidence investigations. Upcoming SAR sensors such as the Japanese Phased Array L-band Synthetic Aperture Radar (PALSAR) onboard the Advanced Land Observing Satellite (ALOS) exemplify a trend towards lower frequencies and higher range chirp bandwidth in order to obtain additional information with higher geometric resolution. However, the use of large bandwidths causes signal degradation within a dispersive medium such as the ionosphere. Under high solar activity conditions at L-band frequencies, ionosphere-induced path delays and Faraday rotation become significant for SAR applications. Due to ionospheric effects, blind use of a generic matched filter causes inaccuracy when correlating the transmitted with the received signal. Maximum correlation occurs where the length of the matched filter, based on a synthetic chirp model of the transmitted signal, is adjusted to correspond to that of the received signal. By searching for the proper adjustment necessary to reach this maximum, the change in length can be estimated and used to derive variations in the total electron content (TEC) and degree of Faraday rotation within the ionosphere from all range lines in a SAR image.

**Keywords:** Synthetic Aperture Radar, Ionosphere, Total Electron Content, Faraday Rotation

## 1. INTRODUCTION

Knowledge of attitude and position of spaceborne SAR sensors has improved in recent years.[1] Concerning geometric accuracy, the importance of atmospheric path delay increases with continuing improvements to the resolution of SAR systems surveying the Earth and other planets. Contributions of atmosphere-induced path delays must be estimated in order to be able to attain a geolocation accuracy independent of atmospheric influences. Atmospheric path delay contributions at L-band frequencies are mainly due to ionospheric influences. In addition to geometry, estimates of Faraday rotation (FR) are necessary to properly calibrate polarimetric data and derived products.
An overview of ionospheric effects and FR is provided in Section 2 and Section 3. Section 4 exemplifies the method -a model of wave radiation for chirp pulses and pulse compression for a SAR system is presented. Section 5 deals with the simulation and theory of an expected chirp shortening under conditions of low and relatively high solar activity conditions. Section 6 shows simulated examples for states of average and high solar activity for both existing and upcoming spaceborne SAR missions. In the last section, limitations, assumptions and conclusions implicit to the method are discussed.

## 2. IONOSPHERIC DELAY

The earth's ionosphere located between the altitudes of approximately 50 - 1500 km, is characterized by the existence of free electrons and ions that influence the refractive index in this area. The degree of ionization is caused mainly by solar UV radiation and depends on the local atmospheric density. The TEC specifies the number of free electrons in a column with a cross section of 1 $m^2$ along the signal path and is defined as[2]

$$TEC = \int_h N_e dh. \tag{1}$$

$N_e$ $[\frac{e}{m^3}]$ is the electron density along the ray path $h$. TEC units (TECU) are defined to be $10^{16}$ electrons per $m^2$. TEC is usually low at night and maximum at round 14:00 local time, when the sun's position is approximately two hours past zenith. The extent of this time shift depends on the time light needs to ionize the layer to the maximum.
Maximum electron density is found in the so called F2-layer of the ionosphere at a height of approximately 350 km. The degree of ionization, i.e. the number of free electrons interacting with the traversing signal, causes a path delay that depends

Remote Sensing of Clouds and the Atmosphere X, edited by Klaus Schäfer, Adolfo Comerón, James R. Slusser, Richard H. Picard, Michel R. Carleer, Nicolaos Sifakis,
Proc. of SPIE Vol. 5979, 59790U, (2005) · 0277-786X/05/$15 · doi: 10.1117/12.627618

mainly on the signal's carrier frequency $f$. This dispersive behavior can be used to estimate the TEC along the ray path. GPS stations, for example, measure the time delay at two frequencies L1 and L2, calculate global TEC over a network of about 200 receiving stations, providing GPS users with ionosphere correction terms through the navigation message. Daily maps of global TEC are published on the Internet (e.g. `www.aiub.unibe.ch/ionosphere/`).
Based on Ref. 3, we can describe the path delay $\Delta s$ through the ionosphere for electromagnetic waves traveling from a satellite to the earth and back by:

$$\Delta s = 2\,K \cdot \frac{TEC}{f^2 \cdot \cos\alpha} \tag{2}$$

$\alpha$ [degrees] denotes the satellite off-nadir angle, and K= 40.28 $[\frac{\mathrm{m}^3}{\mathrm{s}^2}]$ is the refractive constant.[3] The factor $\frac{1}{\cos\alpha}$ accounts approximately for the slant range direction. The quadratic dependency on frequency term indicates that increasingly significant path delays occur at lower frequencies. **Table 1** shows expected path delays at L-band for average and high solar conditions. For an incidence angle of 39 degrees, path delays at C-band are between 2 m and 5.5 m and between 0.5 m to 1.5 m for X-band. **Figure 1** shows mean levels at 13:00 h UTC of global vertical TEC for 1998 and 2002. The maps were calculated using the global ionospheric maps (GIM) from the International GPS Service (IGS). TEC level estimates are sampled every 5 degrees in longitude and 2.5 degrees in latitude.[2]

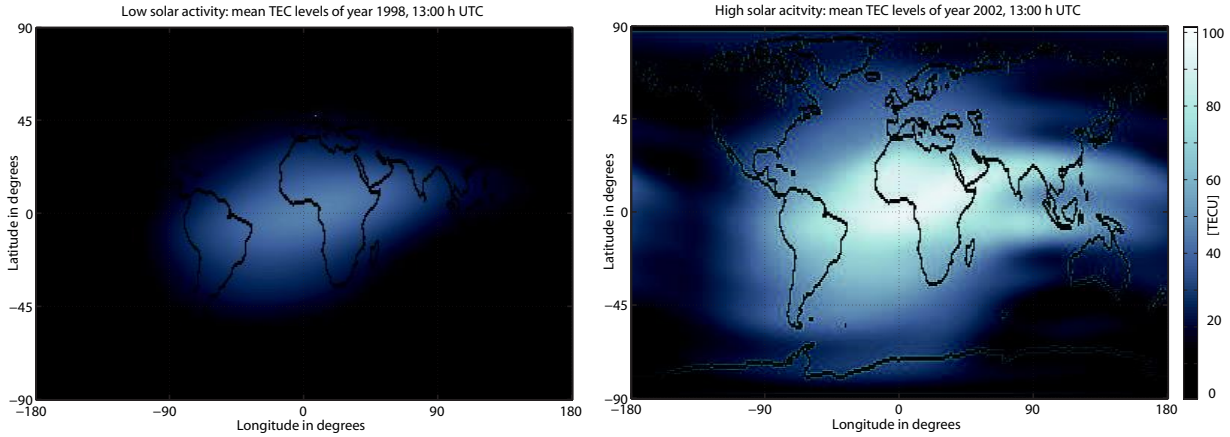


**Figure 1.** Mean TEC levels calculated by averaging 365 GIMs obtained from the IGS. Left: 1998, 13:00 h with average solar conditions. Right: 2002, 13:00 h where TEC levels were around solar maximum.

## 3. FARADAY ROTATION

In addition to the ionosphere-induced path delay described above, which manifests itself as a range shift in spaceborne SAR images, the ionosphere also induces a small polarization-dependent effect which can become significant at L-band or lower frequencies. The free electrons of the ionosphere interact with the traversing electromagnetic wave resulting in a rotation $\Omega$ of the polarization vector. When a linearly polarized wave enters an ionized medium in the presence of an external magnetic field, one can treat the radar wave as split into two oppositely rotating circularly polarized waves traveling at slightly different velocities and along slightly different ray paths. When the two components recombine at the satellite or reach the ground, the resultant linear polarization is different from the initial value.[4] Given the knowledge of local TEC levels and a model of the earth's magnetic field B (e.g. CO2-model[5]), the degree of Faraday rotation FR can be estimated using[6,7]:

$$\begin{aligned} \Omega &= \frac{2.365 \cdot 10^4}{c^2} \cdot \lambda^2 \int_0^h N_e \cdot B \cos\theta \sec\alpha \; dh \\ &= 2.610^{-13} \cdot TEC \cdot B \cdot \lambda^2 \cos\theta \qquad ,\alpha = 0 \end{aligned} \tag{3}$$

where $\lambda$ [m] is the wavelength of the electromagnetic wave and $\theta$ [degrees] is the angle between the magnetic field and the

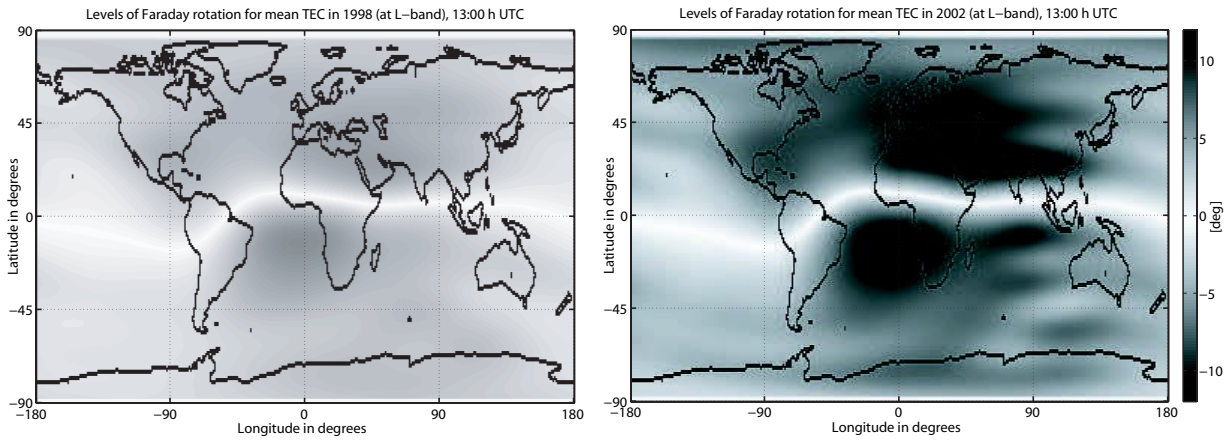


**Figure 2.** Typical levels of one-way Faraday rotation at low and high solar conditions. Based on the calculated mean TEC levels for 1998 and 2002 in Section 2 (see Figure 1) Faraday rotation and the magnetic field is estimated each with day of year (DOY) 202 and vertical incidence angle.

radar wave. $\alpha$ is set to zero for vertical incidence relative to the earth center. Equation (3) refers to one-way propagation through the ionosphere. For SAR applications the effect doubles.[6]

Current TEC estimation methods use a Global Navigation Satellite System (GNSS) network to derive TEC maps together with a magnetic field model to predict FR. **Figure 2** shows estimated FR at L-band for average and high solar conditions in 1998 and 2002. For every pixel the incidence angle relative to the earth center is vertical. To estimate the influence of the ionosphere under low and high solar conditions the mean TEC maps from Figure 1 were used. The magnetic field component was calculated for a height of 100 to 450 km from the CHAMP/Ørsted/Ørsted-2 model (CO2-model[5]) for July 21, 1998 and July 21, 2002, respectively. It is clearly visible that under high solar conditions FR can limit polarimetric analysis in mid-latitude regions.

Another widely used method can be applied when the sensor has a fully polarimetric mode by making use of the fact that backscatter measurement reciprocity (HV=VH) is violated in the presence of FR. By comparing the cross-polarized terms of the scattering matrix,[8] an estimate of the degree of FR may be made. This method has the advantage of not requiring data from outside the sensor environment - however the satellite must acquire the data in full polarimetric mode (full scattering matrix).

## 4. FREQUENCY MODULATION

Spaceborne imaging radar systems transmit modulated pulses to improve resolution in range at a manageable peak power. The most commonly used method is a linear frequency modulation of the transmitted pulse $s_t$, (called a chirp), which is a sine wave with constantly increasing (up-chirp) or decreasing (down-chirp) frequency during its pulse duration. **Figure 3**(a) and (b) show a down-chirp in time and frequency plots. The chirp pulse was simulated using JERS-1 parameters from Table 1.The following two subfigures show the chirp pulse after baseband conversion in time (Figure 3(c)) and frequency domains (Figure 3(d)) respectively. After conversion to baseband the chirp shows symmetry at about half of the pulse length in time and about 0 Hz in the frequency domain (Figure 3(d)). For illustrative reasons (c) shows only a segment from the whole pulse. A discrimination between up- and down-chirps from Figure 3(c) and (d) is no longer possible. With a start frequency $f_{start}$ of

$$f_{start} = f_c + B/2 \tag{4}$$

and a stop frequency $f_{stop}$ of

$$f_{stop} = f_c - B/2 \tag{5}$$

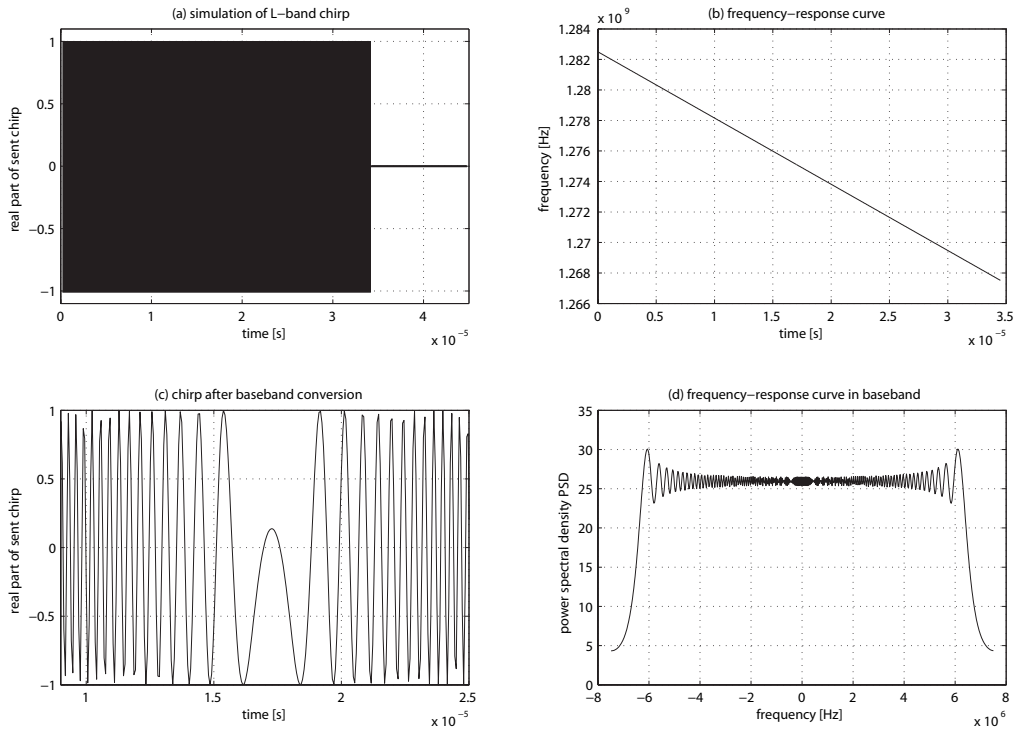


**Figure 3.** (a) Simulated JERS-1 chirp pulse in time domain. (b) plot illustrating the chirp's frequency-dependency on time. (c) chirp pulse in baseband. Pulse form is symmetric about half of the pulse duration. For illustrative purposes, only half of the pulse duration is shown. (d) Power spectrum of baseband converted chirp pulse.

which are located half the bandwidth $B$ off the chirp's carrier frequency $f_c$, a chirp can be written as:

$$\begin{aligned} s_t(t, T_t) &= U_t \cdot e^{j2\pi(f_{\text{start}} t + k_t t^2)} \cdot \text{rect}[0, T_t] \\ k_t &= -\frac{B}{2T_t} \end{aligned} \tag{6}$$

| | | |
|---|---|---|
| $U_t$ | amplitude of the transmitted signal | |
| $k_t$ | chirp rate | [1/s$^2$] |
| $T_t$ | chirp duration of the transmitted pulse | [s] |
| $rect[0, T_t]$ | square pulse of amplitude 1 and length $T_t$ | [unitless] |

From (6) the phase of the chirp waveform is given as

$$\phi(t) = 2\pi \left( f_{\text{start}} t + k_t t^2 \right). \tag{7}$$

The instantaneous frequency of the chirp can then be calculated by

$$f(t) = \frac{1}{2\pi} \frac{d\phi(t)}{dt} = f_{\text{start}} + 2k_t t. \tag{8}$$

The received signal $s_r(t)$ at the antenna can be written as:

$$s_r(t, T_r) = U_r \cdot e^{j2\pi(f_r t + k_r t^2)} \cdot \text{rect}[0, T_r]. \tag{9}$$

with

| | | |
|---|---|---|
| $U_r$ | amplitude of the received signal | |
| $f_r$ | starting frequency of the received chirp | [Hz] |
| $k_r$ | chirp rate of received signal | [1/s$^2$] |
| $T_r$ | chirp duration for the received signal | [s] |
| $rect[0, T_r]$ | rectangular pulse of amplitude 1 and length $T_r$ | [unitless] |

To focus a radar image along a range line the received frequency modulated pulses at the antenna are first down-converted to baseband. They are then compressed through matched filtering. This corresponds to convolution of the measured signal with the complex conjugate of the transmitted chirp $s_t^*$. Mathematically, a convolution is the cross correlation function (CCF) of time reversed i.e. complex conjugate signals. For range compression for the matched filter one has:

$$\begin{aligned} CCF(T_t, T_r) &= s_t^*(t, T_t) * s_r(t, T_r) \\ &= \frac{1}{max\{T_t, T_r\}} \cdot \int_{-max\{T_t,T_r\}/2}^{max\{T_t,T_r\}/2} s_t^*(t, T_t) \cdot s_r(t + \tau, T_r) dt \\ &= \mathcal{F}^{-1}\{S_t(w)^* \cdot S_r(w)\} \end{aligned} \tag{10}$$

As shown above a computationally efficient method to solve this equation is to calculate the product of the signals in the frequency domain and estimate the CCF in time-domain over the inverse Fourier transform.

## 5. SIMULATION OF CHIRP SHORTENING

The principle of a matched filter as described in Section 4 is sketched in **Figure 4**. The frequency modulated transmitted signal is compared with the received chirp signal of a point target. Simulating an up-chirp, the received signal is shortened

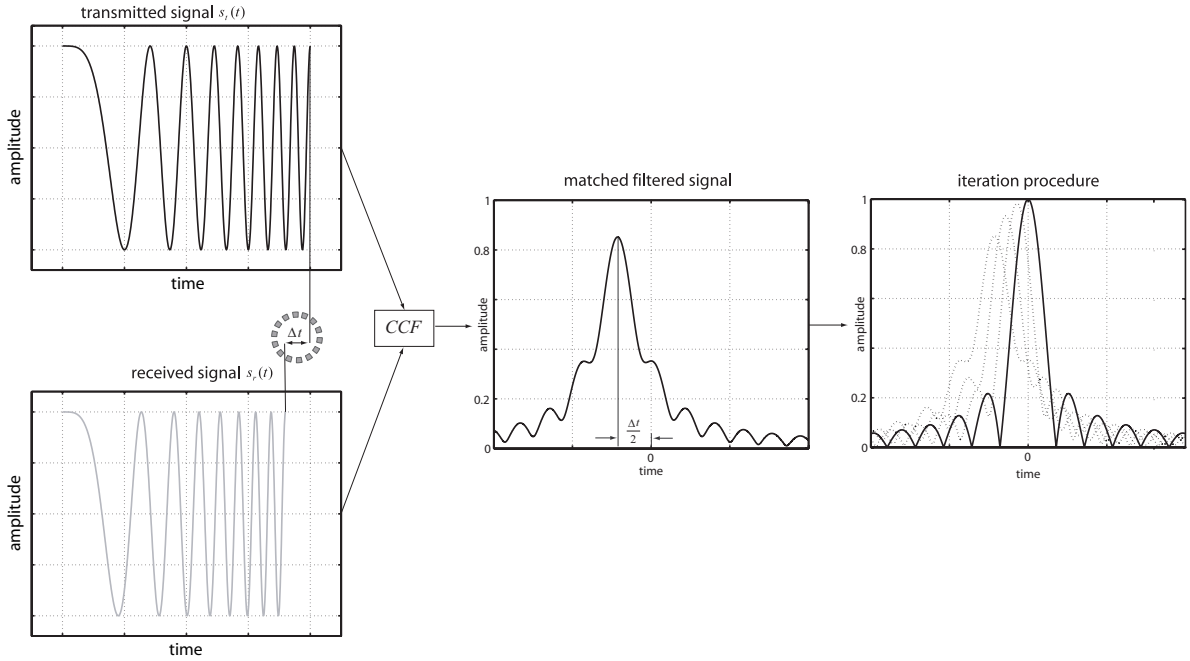


**Figure 4.** Simulated correlation of two chirps. The chirps, differing in pulse duration correlate suboptimally and appear defocused and shifted. An iterative procedure correlates within an interval defined by the range of expected TEC until a maximum correlation is found.

because higher frequency chirp segments return slightly faster to the satellite antenna than lower frequency parts that are delayed slightly longer in the ionosphere. Comparing transmitted vs. received pulses the shortening influences neither the bandwidth nor the start and stop frequency of the transmitted pulse but does change the chirp rate $k$.
Concerning range resolution, the reflected signal passes through a filter that delays it to an extent that is a function of frequency. As mentioned above the filter function corresponds to the cross correlation of the transmitted signal with the received signal. To obtain maximum correlation, it is necessary to know both the *chirp rate* and *duration* of the received signal. In conventional SAR applications the filter function is implemented using the autocorrelation, implicitly assuming that the form of the received chirp signal corresponds exactly to that of the transmitted chirp. Signals influenced by the ionosphere correlate suboptimally and may appear defocused and shifted in range. A way to solve this problem is to modify the synthesized reference transmit signal before correlating so that a maximum correlation is achieved. One can change the length of the pulse duration of the transmitted chirp in steps of $\Delta t$ to find

$$CFF(\Delta t_{TEC}) = max\{CCF(T_t + n \cdot \Delta t, T_r)\} \qquad \text{with} \quad n \quad \epsilon \quad [n_{\text{min}}, n_{\text{max}}] \tag{11}$$

where $n_{\text{min}}$ and $n_{\text{max}}$ delimit the search space, and

$$\Delta t(n_{\text{max}} - n_{\text{min}}) \tag{12}$$

covers the entire theoretically possible shortening time range. $\Delta t_{TEC}$ represents the time delay from the synthesised transmitted chirp at which a maximum in correlation is reached.
Referring to Section 2, path delays caused by the ionosphere depend on the TEC and on the carrier frequency according to (2). The higher the bandwidth and the lower the carrier frequency of the chirp the more significant the change in length of the received chirp becomes. The ionosphere's dispersive behavior shortens a transmitted up-chirp; down-chirps are broadened. An estimated change in length $\Delta t_{TEC}$ within the pulse duration of a chirp may be used to estimate the TEC value along the ray path:

$$TEC = \frac{1}{2} \cdot \frac{\Delta t_{TEC} \cdot c}{K} \cdot \left( \frac{f_{start}^2 \cdot f_{stop}^2}{f_{start}^2 - f_{stop}^2} \right) \tag{13}$$

In order to illustrate the behavior of the maximum in correlation over different chirp lengths, **Figure 5** illustrates a distribution with two simulated chirps. The properties for the chirps were again chosen for the JERS-1 case (down-chirp at L-band). One chirp is set to constant length and duration and simulates the received chirp. The other changes its length and chirp rate from shorter to longer. Figure 5(a) shows an example given that the signal passed the ionosphere without

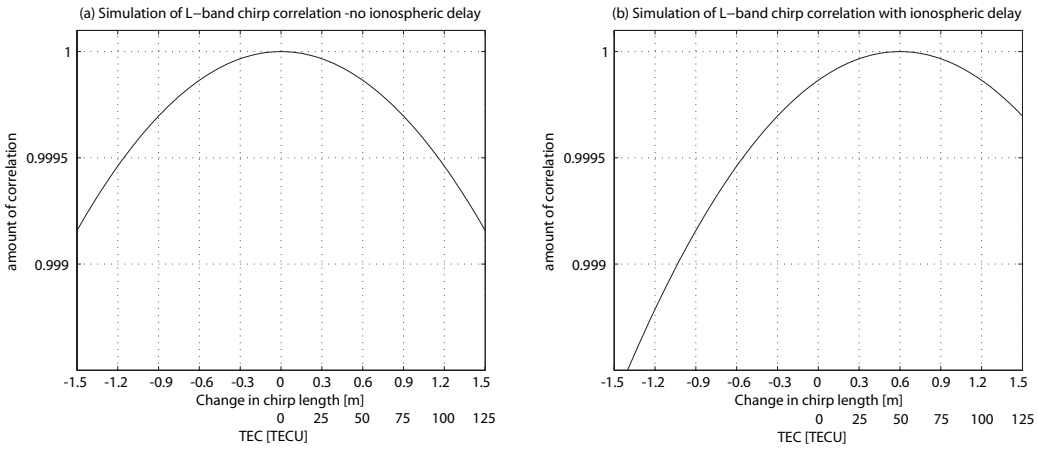


**Figure 5.** Simulation of maxima in correlation for two chirps, where one is set to a constant chirp length and the other is shortened. (a) assumes that the ionosphere has no influence on the chirp length. (b) assuming that the received chirp was broadened.

any change to its length. As expected, correlation is highest when the lengths of the two chirps are equal at 0 TEC, where no difference in length and chirp rate is expected. In a situation where the received chirp is broadened, e.g. due to a TEC of 50, the absolute maximum in the graph of Figure 5(b) shifts to higher TEC values on the right.

## 6. SIMULATION FOR SPACEBORNE L-BAND SAR SENSORS

As mentioned previously, radar systems at L-band or lower frequency are strongly affected by the ionosphere. Data for analysis is rare or currently not adequate for accurate examination. In the following, a 3D-simulation for a point target with reference sensor configurations was made to give an impression of how spaceborne SAR sensors can be affected under relatively high and normal ionospheric conditions. Interesting sensor configurations are JERS-1, ALOS PALSAR and TerraSAR-L -all operating at L-band, with a broad range of bandwidths. Table 1 shows details for the respective sensors. A detailed description of the system model is available in Ref. 9.

| **Sensor** | **Units** | **TerraSAR-L** | | | **ALOS PALSAR** | | | **JERS-1** | | |
|---|---|---|---|---|---|---|---|---|---|---|
| Frequency ($f_c$) | [GHz] | 1.2575 | | | 1.27 | | | 1.275 | | |
| Range bandwidth B | [MHz] | 85 | | | 28 | | | 15 | | |
| Chirp duration | [$\mu$sec] | 35 | | | 28 | | | 35 | | |
| Sampling rate | [MHz] | 102* | | | 33.6* | | | 17.1 | | |
| Chirp form | | Upchirp | | | Downchirp | | | Downchirp | | |
| Orbit (altitude) | [km] | 629 | | | 695 | | | 580 | | |
| Simulated TEC | [TECU] | 0 | 60 | 150 | 0 | 60 | 150 | 0 | 60 | 150 |
| Off-nadir $\alpha$ | [deg.] | 39 | 39 | 39 | 39 | 39 | 39 | 39 | 39 | 39 |
| Path delay at $f_c$ (2-way) | [m] | 0 | 39.3 | 98.3 | 0 | 38.6 | 96.4 | 0 | 36.4 | 91.0 |
| Change in received chirp length | [m] | 0 | -5.33 | -13.32 | 0 | 1.7 | 4.25 | 0 | 0.86 | 2.14 |
| 3 dB width | [m] | 2.13 | 4.71 | 12.48 | 6.45 | 6.47 | 6.54 | 12.05 | 12.05 | 12.06 |
| Difference in amplitude $\Delta t$=0 vs. $\Delta t_{\max}$ | [dB] | 0 | -1.13 | -5.68 | 0 | 0.013 | -0.076 | 0 | -0.001 | -0.007 |
| Peak sidelobe ratio (PSLR) | [dB] | -6.63 | -6.20 | -1.76 | -6.63 | -6.57 | -6.24 | -6.63 | -6.63 | -6.61 |

*Sampling rates for TerraSAR-L and ALOS PALSAR were assumed using typical oversampling factors.

**Table 1.** Satellite sensor details and estimates of influence of 0, 60, 150 TECU on the path delay, the 3 dB bandwidth, amplitude and PSLR, based on simulations.

### 6.1. TerraSAR-L

With a possible launch after 2006, a low center frequency, and a high bandwidth for a SAR-system, the returned signals

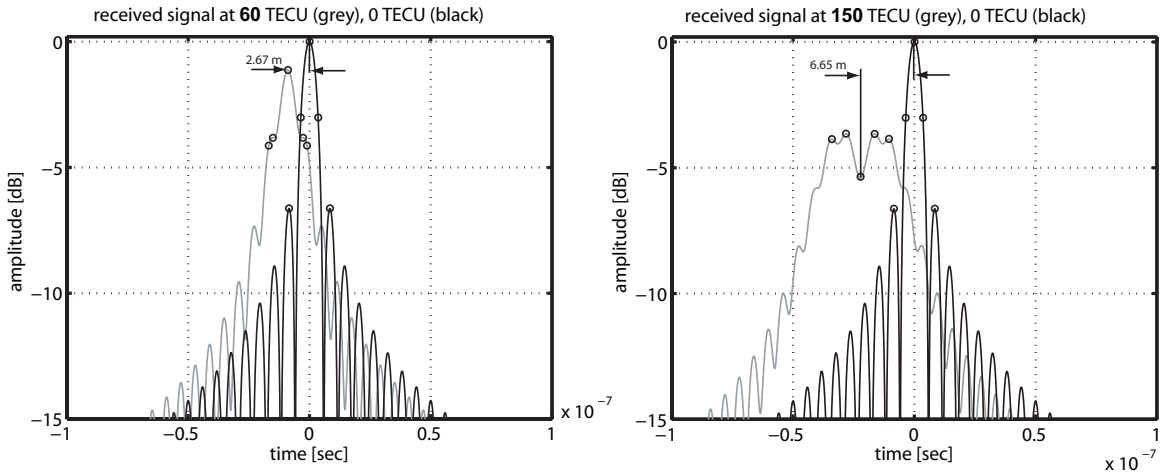


**Figure 6.** Simulated response function of cross correlation for TerraSAR-L at 60 and 150 TECU.

of TerraSAR-L as simulated in **Figure 6** would be expected to degrade extremely under high solar conditions. Simulation assuming 150 TECU shows that the uncompensated 3 dB bandwidth spreads to over 12 m.

### 6.2. ALOS PALSAR

**Figure 7** shows results of simulations based on ALOS PALSAR parameters. PALSAR, a SAR system at L-band frequency with smaller bandwidth and a launch planned in late 2005 should have less degradation in resolution. At L-band frequencies, the system should be capable of detecting ionospheric changes with a sensitivity that depends on the sensors sampling frequency.

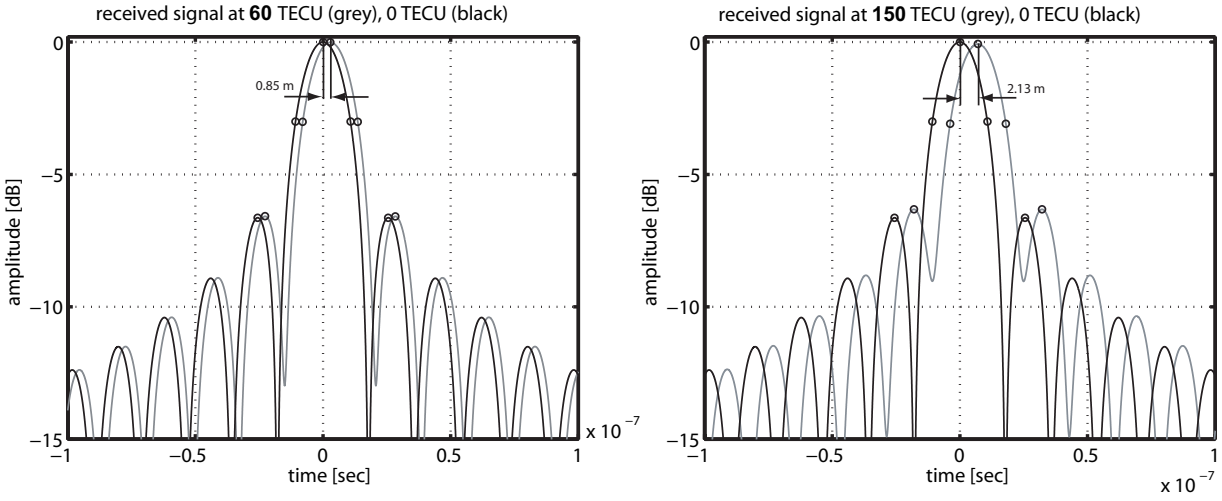


**Figure 7.** Simulated response function of the cross correlation for ALOS PALSAR at 60 and 150 TECU.

### 6.3. JERS-1 (1992 - 1998)

**Figure 8** shows because of a relatively low bandwidth compared to ALOS and TerraSAR-L, TEC estimation with JERS-1 is made more difficult. A limiting factor for the detection of TEC at 5 TECU sensitivity is the 17 MHz sampling rate. The

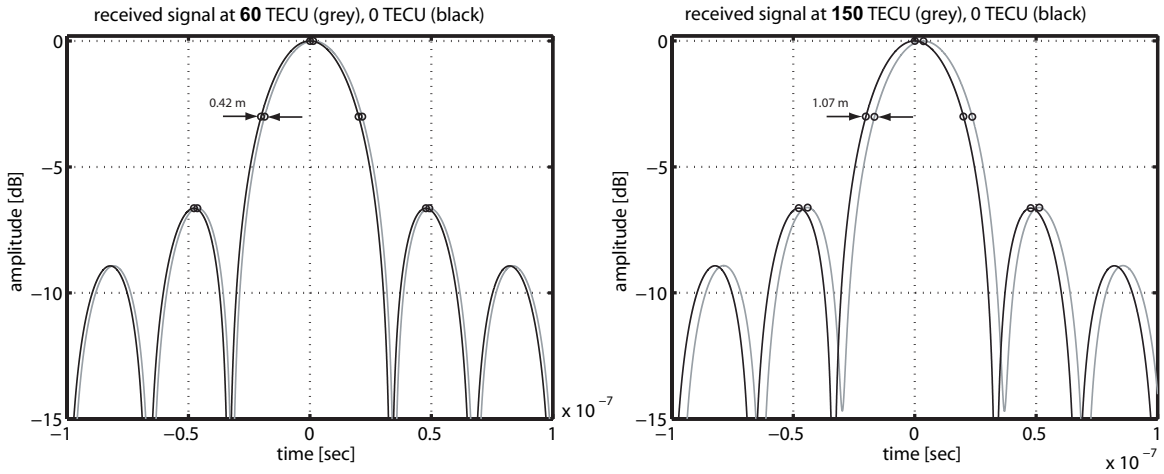


**Figure 8.** Simulated response function of the cross correlation for JERS-1 at 60 and 150 TECU.

small 15 MHz bandwidth causes relatively small changes in chirp length, close to practicable detection limits.

## 7. CONCLUSION

High resolution spaceborne SAR sensors such as the upcoming PALSAR on ALOS provide possibilities for detecting slant path delays of electromagnetic wave propagation through the ionosphere. Caused by the frequency dependent runtime of a radar signal through the ionosphere, the change in length of a chirp signal could be measured by searching for the proper adjustment necessary to reach a maximum in correlation of the transmitted and received signal. Simulations of ALOS, TerraSAR-L and JERS-1 show that an estimation of TEC levels within each range line of a SAR scene with a sensitivity of approximately 5 TECU might be possible. First results with JERS-1 data show good agreement with values derived from global GPS-TEC maps and motivate further investigations. Extracting TEC levels from spaceborne SAR sensors or other radar instruments such as altimeters which use chirp-like waveforms could provide support for future estimates of Faraday rotation, antenna range biases or slant mapping of TEC values. SAR-derived TEC levels can be used for an autonomous calibration of ionospheric effects on SAR images. Limitations are set by the respective sensor sampling frequencies, the chirp bandwidth and the overlying noise.

## REFERENCES


1. D. Small, B. Rosich, A. Schubert, E. Meier, and D. Nüesch, "Geometric Validation of Low and High-Resolution ASAR Imagery," *Proceedings of the 2004 Envisat and ERS Symposium* **ESA SP-572**, p. 9, Apr. 2005.
2. S. Schaer, "Mapping and Predicting the Earth's Ionosphere Using the Global Positioning System," *Geodätisch-geophysikalische Arbeiten in der Schweiz* **59**, 1999.
3. R. F. Hanssen, *Radar Interferometry.*, vol. 2, Kluwer Academic Publishers, 2001.
4. R. Fitzpatrick, "Faraday Rotation." `http://farside.ph.utexas.edu/teaching/em/lectures/node101.html`, 2005.
5. R. Holme, "CO2-A CHAMP magnetic field model." `http://www.dsri.dk/Oersted/Field_models/CO2/`.
6. P. A. Wright, S. Quegan, N. S. Wheadon, and C. D. Hall, "Faraday Rotation Effects on L-Band Spaceborne Data.," *IEEE Transactions on Geoscience and Remote Sensing* **41**, pp. 2735–2744, Dec. 2003.
7. E. J. M. Rignot, "Effect of Faraday Rotation on L-Band Interferometric and Polarimetric Synthetic-Aperture Radar Data.," *IEEE Transactions on Geoscience and Remote Sensing* **38**, pp. 383–390, Dec. 2000.
8. A. Freeman, "Calibration of Linearly Polarized Polarimatric SAR Data Subject to Faraday Rotation," *IEEE Transactions on Geoscience and Remote Sensing* **42**, pp. 1617–1624, Aug. 2004.
9. M. Soumekh, *Synthetic Aperture Radar Signal Processing.*, vol. 1, John Wiley & Sons, Inc., 1999.